Interventional cardiac MRI using an add-on Parallel Transmit MR system: *In vivo* experience in sheep

Running head: Interventional MRI using an add-on PTx MR system with current sensor feedback

Felipe Godinez[1,2], Raphael Tomi-Tricot[3], Marylène Delcey[4,5], Ronald Mooiweer[1], Steven E Williams[1], Bruno Quesson[4], Reza Razavi[1], Joseph V Hajnal[1,2], and Shaihan J Malik[1,2]

[1]School of Biomedical Engineering and Imaging Sciences, King's College London, London, United Kingdom
[2]Centre for the Developing Brain, School of Biomedical Engineering and Imaging Sciences, King's College London, London, United Kingdom
[3]MR Research Collaborations, Siemens Healthcare Limited, Frimley, United Kingdom
[4]Centre de Recherche Cardio-Thoracique de Bordeaux/IHU Liryc, INSERM U1045-University of Bordeaux, Pessac, France
[5]Siemens Healthcare, France, F-93210 Saint-Denis, France

Corresponding Author:
Felipe Godinez, PhD
1st Floor South Wing
St Thomas' Hospital
Tel: +4407521229754
Email: felipe.godinez@kcl.ac.uk

Abstract

Purpose: We present in vivo testing of a parallel transmit (pTx) system intended for interventional MR-guided cardiac procedures.

Methods: The pTx system was connected in-line with a conventional 1.5T MRI system to transmit and receive on an 8-coil array. The system used a current sensor for real-time feedback to achieve real-time current control, by determining coupling and null modes. Experiments were conducted on 4 Charmoise sheep weighing 33.9-45.0kg with nitinol guidewires placed under x-ray fluoroscopy in the atrium or ventricle of the heart via the femoral vein. Heating tests were done, in vivo and post-mortem, with a high RF power imaging sequence using the coupling mode. Anatomical imaging was done using a combination of null modes optimized to produce a useable B1 field in the heart.

Results: Anatomical imaging produced cine images of the heart comparable in quality to imaging with the quad mode (all channels with the same amplitude and phase). Maximum observed temperature increases occurred when insulation was stripped from the wire tip. These were 4.1°C and 0.4°C for the coupling mode and null modes respectively in-vivo, increasing to 6.0°C and 1.3°C respectively ex-vivo since cooling from blood-flow is removed. Heating <0.1°C was observed when insulation was not stripped from guidewire tips. In all tests the pTx system managed to reduce the temperature at the guidewire tip.

Conclusion: We have demonstrated the first in vivo usage of an auxiliary pTx system employing active feedback based current control for interventional MRI with a conventional MRI scanner.

Keywords: Auxiliary pTx system, Interventional MRI, MR-guided catheterization, Guidewire visualization, Cardiac Catheters, Medical device heating, Real-time MRI, Invasive hemodynamics, Parallel Transmit MRI

1. Introduction

Metallic interventional devices pose a risk in MRI because they are susceptible to radiofrequency (RF)-induced currents which can produce dangerous tissue heating (1–3). Additionally, visualizing standard guidewires with MRI is difficult. Together, these factors present substantial obstacles to MRI-guided cardiovascular interventions. This is unfortunate considering that MRI provides improved soft-tissue contrast, can provide functional measures such as flow and eliminates radiation dose (4,5). Similar risks of RF induced heating are present for any elongated conductive device used in cardiac interventions including guidewires, exchange wires, or braided catheters.

Many approaches have been proposed to solve the two major challenges of guidewire safety and visualization for interventional procedures. Regarding safety, low RF power (6) or lower B_0 field strength (i.e. lower frequency) systems (7) have been used. Operating at low power in a conventional MRI scanner can provide a safety margin, but with trade-offs in imaging performance required for visualization of both anatomy and guidewires (6). Low field-strength scanners are a promising alternative but are not widely available. Alternatively, devices made from materials such as plastic or fiberglass have been investigated (8). While reducing the risk from heating these may not have suitable mechanical properties for all types of intervention. For visualization, a range of approaches are possible including the use of susceptibility-related effects (9,10), auxiliary contrast markers (11,12), or some form of a local signal detector mounted on or integrated into the device (13–15). In like manner, detecting signal at the device tip has been achieved by modifying guidewires with active components (12,16,17), but these modification approaches require development of bespoke interventional devices.

The physical mechanism responsible for unsafe RF-induced currents is RF coupling between transmit coils and the guidewire. This depends on both the electric field tangential to the guidewire and the sensitivity of the wire to transfer energy to the tip, both of which are spatially varying in magnitude and phase (2,18,19). Adjustment of the spatial distribution of incident electric field is not possible with a conventional single channel transmit MRI system, but can be achieved using parallel transmission (pTx) (20,21). For interventional work, Gudino et al (21) demonstrated this *in vivo* using simulated RF fields to predict and therefore minimize induced currents based on knowledge of the path of a wire through space. Etezadi-Amoli (20) et al presented a framework for computing safe modes for excitation using current

sensor measurements that can be made in real-time. The advantage of this second approach is that it allows for an active feedback mechanism that is independent of the imaging being undertaken. This is important because the coupling depends on details of the device including the length (especially the inserted length), diameter and presence or absence of electrical insulation (22,23). Furthermore, during a typical procedure, such as in cardiac interventions, the insertion length and location of the guidewire are constantly changing, suggesting the need for an active and real-time RF-induced current control system.

Following Etezadi-Amoli et al, if the coupling between each transmit coil element and the guidewire can be quantified, then a series of pTx operation 'modes' can be defined. These can be classified as either 'coupling modes' (CM) which induce currents in the guidewire or 'null current modes' (NM) which null currents (20,24,25) at the point of measurement. Although these modes can generate/null currents, they do generate RF magnetic fields (B_1^+), and so can allow MRI to proceed, but with very different safety profiles(26). NMs restrict RF-induced currents well in MR imaging of deep brain stimulators (24,25,27) and guidewires (21). In contrast, the CMs can produce dangerously high guidewire currents that are usually not used for imaging. However coupling modes can enhance the transmit fields adjacent to the guidewire, and so by working at ultra-low transmit amplitude CMs can be used for safe device visualization (26,27). A similar effect has been achieved using birdcage coils (28).

Aside from 2-channel birdcage devices used by modern 3T MRI systems, commercial pTx systems are typically restricted to ultrahigh field MRI. However investigational pTx systems have been described in literature (29–31). We have designed and built an 'auxiliary' active pTx device that can be used to augment a standard MRI scanner, enabling 8-channel transmission with dynamic control of CM and NM achieved through real-time measurement of currents on inserted guidewires (32). In this work we describe first experience of deploying this device for interventional cardiac MRI using standard guidewires in an *in vivo* sheep model including both safety assessment and device visualization.

2. Methods

2.1 Design overview and implementation

This study was carried out using an unmodified 1.5T system (MAGNETOM Aera, Siemens Healthcare, Erlangen, Germany). A schematic diagram of the dynamic auxiliary pTx system, which is described in full in (32) is shown in Figure 1. In the brief, the pTx system receives the scanner's high-power RF output, attenuates and splits this into eight parallel channels with equal amplitudes. It then uses low power vector modulation to implement per-channel amplitude and phase control before re-amplification by a bank of eight RF power amplifiers (RFPAs).

Real-time monitoring of the RF-induced currents into the guidewire was achieved using an inductively coupled toroidal current sensor (33). The sensor was built from 1 mm diameter transformer wire coiled in the long-axis direction through a 5 mm diameter plastic tube, providing space for the guidewire to pass through the tube Figure 1B. The sensor was wrapped with copper foil to block incident RF energy and a 10m shielded balanced twin-pair line was attached to the coil and connected to a balun. This same sensor was also used for direct excitation of the guidewire in some experiments, described later.

The auxiliary pTx system was controlled using a bespoke MatLab (MathWorks Inc, MA, USA) based user interface (see Supporting Information Figure S1) running on a PC, which also acted as a data logger recording guidewire currents. This architecture facilitated mode updates between individual RF pulses, but as it was asynchronous and interrupt based it did not provide full dynamic pTx (34), which was not necessary for our application.

Key requirements for the pTx system as a whole were:

1. To control the modes of coupling actively and continuously to the guidewire while operating transparent to the scanner, so that the scanner maintains all functionality and control over the transmit RF-signal. This was achieved by ensuring the total pTx system gain (from coil connector to transmit array) had a default value of unity.
2. To require minimal physical connections to an unmodified scanner (see Figure 1a). The system connected to a standard RF output available on the MRI scanner bed via the Total imaging matrix (Tim) plug intended to connect to local transmit coils. Other essential

connections were the RF amplifier unblanking signal, which is located under a removable cover, and an optic-fiber trigger pulse that is typically used for functional MRI.

The custom-built transceiver 8-channel surface coil array used (RAPID Biomedical, Rimpar, Germany) was composed of three main parts: an interface box and two surface arrays (anterior and posterior) each consisting of four coil elements (33). The interface box was connected to the scanner's Tim adaptors and handled routing of the outgoing high-power RF signal and returning (modulated and re-amplified) per-channel pTx RF signals.

2.2 MRI sequence integration

2.2.1 RF-Coupling Measurement

A detailed description of the RF-coupling measurement can be found in (20). In short, a coil-to-guidewire coupling matrix **C** is required to compute the system RF-coupling mode. It is measured frequently during any invasive procedure, to account for potential changes in RF-coupling. This is achieved by adding an off-resonance pulse (to avoid interacting directly with the magnetization) into a chosen target pulse sequence. An example is illustrated in Figure 2, which shows a single-shot turbo spin echo (ssTSE) sequence modified by adding a trigger event followed by 20ms rectangular pulse with amplitude 40V and frequency offset 5kHz (parameters can be set on the scanner console). On receiving the trigger, the pTx system sets all channels to zero output power, commencing the measuring cycle during the 5kHz rectangular pulse, which cycles through the transmit channels one at a time while the digitizer records the resulting current-sensor signal to obtain **C**.

Singular value decomposition of **C** results in a matrix **V** of right singular vectors which specify the required operational modes (20). For measurements from *n* current sensors the first *n* columns of **V** correspond to per-channel weightings (RF-shims) for the CMs; the remaining columns form matrix $\widetilde{\boldsymbol{V}}$ and define the NMs (26). Depending on the choices made within the software, a new RF-shim computed from updated **C** can be immediately applied to the subsequent RF pulses, or simply logged, with a maximum update time of 50ms. For the experiments reported this type of measurement was integrated into a ssTSE sequence, which was used for guidewire visualization using CM excitation (26), and a balanced Steady-State-Free-Precession (bSSFP) sequence for anatomical imaging, usually exploiting NM. For ssTSE,

one measurement event was used per TR; for bSSFP, events were included at a frequency of once per full image frame to avoid interrupting the steady state too often.

2.2.2 RF-shimming using null modes

Safe guidewire imaging can be achieved using any linear combination of the NMs; a combination that also yields good B_1^+ homogeneity and respects per-channel peak power limits can be calculated as described in (26). The RF shim calculation requires B_1^+ maps for each coil in the array and these were obtained as described below (section 2.3.1). The result of this calculation is a complex vector of weights, **w**, to be applied to each channel. Previous work described a 'static' scenario in which **w** is not dynamically updated. In this work, for real-time RF-induced current nulling, **w** must be updated regularly and potentially at the same rate at which **C** is updated, as **C** will change as the guidewire is manipulated. Recomputing **w** can take several seconds, instead a real-time RF shim $\boldsymbol{w_{rt}}$ is rapidly estimated from the optimal RF shim, using the most recently determined set of NMs $\widetilde{\boldsymbol{V}}_{\boldsymbol{rt}}$:

$$\boldsymbol{w_{rt}} = \widetilde{\boldsymbol{V}}_{\boldsymbol{rt}}\widetilde{\boldsymbol{V}}_{\boldsymbol{rt}}^{\boldsymbol{H}}\boldsymbol{w} \qquad [3]$$

This is guaranteed to yield a safe combination according to the newly updated coupling measurement but not necessarily yield an optimally uniform B_1^+ field; safety is prioritized. The software was configured such that either option is possible, the intention being that during a slow period (guidewire is inserted into the body but not actively manipulated) a full calculation of $\boldsymbol{w}$ can be performed, while during active manipulation the real-time updates continue to maintain safety by using $\boldsymbol{w_{rt}}$.

2.3 Experiments

Imaging experiments were performed on phantoms and an animal model. All experiments involved the use of a single standard nitinol guidewire with a polyurethane outer coating of 0.89mm diameter (RF+GA35153M, Terumo Corporation, Japan). In some of these experiments, the coating was stripped from the tip of the guidewire (~2mm exposed) and the guidewire length itself was trimmed, to enhance potential heating effects (details below). All other devices such as the introducer sheath was made of plastic only, such that the guidewire was the only potential source of heating and was the focus for all measurements. In all cases,

a single current-sensor was used, located externally within 10cm of the entry point of the guidewire into the phantom or body of the animal.

Throughout all MR experiments, the temperature at the tip of the guidewire was monitored using a fiber-optic temperature probe (LumaSense Technologies, Inc. USA). The optic fiber was attached at several locations to the guidewire with nylon thread such that the temperature sensor was flush with the guidewire tip. The guidewire tip was selected for temperature monitoring since it is accepted from the literature that this would be the site for worst-case heating (24,35,36).

2.3.1 MR imaging protocols

For piloting, the pTx system was operated in a pre-defined quadrature mode (quad) where each channel has the same amplitude and a fixed phase relationship. At the start of the imaging session for each intervention, per coil B_1^+ mapping was performed using pre-saturated TurboFLASH (37) with two averages; this is a standard vendor sequence but was modified such that the B_1^+-encoding saturation and the imaging readout pulse could be cycled between channels of the pTx system. To ensure sufficient signal in each imaging acquisition, all channels were activated in an 'interferometric' approach (38) instead of activating only one channel per acquisition. Trigger pulses were added to the sequence to signal to the pTx system to switch RF-shim as required. Since neither the coil nor the subject was moved during the MRI guided procedure experiments, it was assumed that these initial field maps would remain pertinent for the entire examination.

A standard bSSFP cine sequence was used for anatomical imaging. This had 1.8mm in-plane resolution and 6mm slice thickness (FOV: 340mmx298mm) with TR/TE 2.70ms/1.16ms, flip angle 44°, 2 signal averages, GRAPPA factor 2 and retrospective cardiac gating with 25 phases, total scan time 29s.

2.3.1.1 In vivo Visualization

Visualization of the guidewire was performed using CM excitation with ssTSE at low net average power as described in (26), the power level was adjusted manually to get the best

visualization result. The ssTSE was demonstrated to provide optimal guidewire visualization as it has a signal profile that is highly sensitive to variations in flip angle (26). The method uses a projection through an 80mm-thick slab. Echo train length of 86, 62% phase partial-Fourier reconstruction, and GRAPPA 2 were used to give a TE of 41ms. A TR of 3000ms was used to prevent saturation effects during in vivo test conditions. The nominal resolution was 1.76mm in plane with a field of view (FOV) of 450mm x 450mm. In phantom experiments, a TR/TE of 300ms/36ms was used.

An alternative method of direct guidewire excitation was also tried. In this case, the current sensor was connected directly to the output of one RFPA. This approach was attempted using the ssTSE sequence just described, and a bSSFP sequence with a variable frequency offset to reduce off-resonance artifacts from air-tissue interfaces. The RF power was adjusted manually to improve image quality.

2.3.2 Phantom experiments

A 14-litre container filled with polyacrylic acid gel made according to the ASTM standard (39) was used to test performance of the pTx system. The properties of the gel were measured as relative permittivity 79.0±1.0 and conductivity 0.531±0.006 Sm^{-1}. A 140cm-long guidewire with stripped tip was placed approximately axially (i.e. in the scanner 'z' direction) into the gel, then exiting the phantom through a hole and trailing along the scanner bed. The short guidewire length was chosen to demonstrate a case of extreme heating. Guidewire visualization as described above was performed in the phantom.

Worst-case heating was demonstrated by running a bSSFP scan at high power for 6 minutes with the following parameters: TR/TE = 3.38ms/1.67ms, FA =70°. In practice the maximum power was limited by the peak on one channel. After each heating acquisition, the temperature returned to baseline. This heating protocol was used in all heating experiments, in phantom, in vivo, and post-mortem.

2.3.4 Animal Study

The major objective of these tests was to validate that the pTx system could operate safely and maintain low temperatures at the tip of a guidewire while also performing structural MRI. The ability of the system to aid visualization of the guidewire was also investigated.

Experiments were performed using a combined MRI and X-ray angiography suite (Artis Zee, Siemens Healthcare, Erlangen, Germany) installed in adjacent rooms. All procedures involving animals were approved by the Animal Research Ethics Committee (CEEA 50 - France) and performed in accordance with the European rules for animal experimentation. Animal experiments were conducted both *in vivo* and *post-mortem* on Charmoise sheep (N=4) weighing 33.9–45.0 kg. The sheep model was selected for having heart dimensions, body weight and physiology similar to humans. Premedication was performed by IM injection of ketamine (10-20 mg/kg, Axience, France), acepromazin (0.1 mg/kg, Vetoquinol, France) and buprenorphine (9 µg/kg, Virbac, France). Anesthesia was then induced with an intravenous injection of propofol (1 mg/kg, Mylan, France) and maintained by oral-tracheal gaseous inhalation (15 breath per minute) of 1-3% Isoflurane (Axience, France) in 50/50 oxygen/air using a MR-compatible ventilator (Aestivia, General Electric, Fairfield, CT, U.S.A). Heart rate, body temperature and blood oximetry were monitored continuously (Maglife, Schiller, France) until completion of the procedure. The subjects were euthanized by lethal IV injection of 80 mg/kg of exagon (Axience, France). After anesthesia was induced, standard nitinol guidewires were inserted using X-ray angiography with access via the femoral vein, into the right ventricle of the heart. Subjects were placed in the supine position for both X-ray insertion and subsequent MR imaging.

2.3.4.1 In vivo Heating

To test different heating scenarios, guidewires of different lengths were used, in some cases with the insulating coating stripped from the tip since this represents a worst-case heating scenario (2). Stripped coating is referred to as a 'stripped tip', while intact insulating coating is referred to as 'insulated tip' from hereon. In subject 1, a shortened guidewire 140cm long with stripped tip was used. This guidewire was inserted with a 60 cm long 13Fr sheath to prevent abrasion or puncture of vessels from the exposed guidewire tip, which was left in place during imaging. In the remaining three subjects, experiments were performed using a standard unmodified guidewire 260cm-long and with an insulated tip (RF-PA35263M, Terumo Europe), or a modified guidewire as detailed in Table 1—the guidewire length was modified to 164cm to account for a longer 96cm long plastic 13Fr sheath. Once the guidewire was in the desired place, the sheath was retracted to expose about 4cm of the guidewire's distal end. In subject 4, the sheath was completely removed after placement of the guidewire in the

right heart ventricle. Exchange of wires was performed under X-ray guidance. Each subject was euthanized after the final imaging experiment to allow for further heating tests to be conducted post-mortem to exclude the effects of blood flow effects on heating.

Table 1 Experimental setup across all subjects. ‘Stripped’ refers to wires with stripped coating at the tip. ‘CM’ refers to visualization using coupled mode excitation, "Direct" refers to use of the current sensor as a transmitter, ‘Pulled out’ refers to removing the sheath after placing the guidewire.

Subject	length	Tip	Visualization	Sheath length
1 45kg	140 cm	stripped	CM	60cm
2 44kg	164 cm	stripped	CM	96cm
3 38kg	260cm	insulated	CM	96cm
	164 cm	stripped	CM/Direct	96cm
4 33kg	164 cm	stripped	CM/Direct	Pulled out

3 Results

3.1 Phantom Tests

A temperature increase of 23.9°C was measured at the guidewire tip inside the gel phantom while operating at CM after 6 minutes of scanning, shown in Figure 3A. In contrast, when operating in the NM at equivalent RF power level, the observed maximal temperature increase was 1.65°C. The measured average total forward power was 40W and 38W for CM and NM, respectively. The visualization of the guidewire using CM excitation and ssTSE sequence is presented in Figure 3B. The average total forward power during the visualization sequence was 2.6W and there was no observable temperature increase.

3.2 In vivo Imaging

Figure 4 illustrates single frames from cine bSSFP images of subjects 3 and 4 in four-chamber view. The ‘quad’ mode image uses the transmit array with predefined and fixed RF-shim between coils (not guaranteed to be safe), while the NM image uses a safe RF-shim consisting

of only NM optimized to produce a uniform excitation in the heart. Acceptable image quality is achievable when only using NMs. The use of a surface array resulted in brighter signal at the surface; note that receive sensitivity correction was not applied. Figure 5 shows measured B_1 maps for subjects 3 and 4.

3.3 In vivo Heating

Table 2 shows the measured temperature at the guidewire tip, taken both in vivo and post-mortem during high-power heating test scans. Reported temperature changes are differences between 30-second averages (see Supporting Information Figure S2 for a full temperature profile) taken immediately before and at the end of each six-minute scan (in subject 1, two-minute scans were used) and the standard deviation of the temperature during this period. Average total power of approximately 100W was used for both NM and CM temperature measurement.

Table 2 Heating measurements. The average temperature change over a 30s period in the plateau region and the standard deviation during this period are shown.

Subject	Guidewire length	Tip condition	Temperature change (°C)			
			In vivo		Post-mortem	
			Coupling	Null	Coupling	Null
1	140	stripped	4.14±0.05	0.38±0.07	6.02±0.06	0.47±0.07
2	164	stripped	0.39±0.17	0.13±0.06	2.14±0.02	0.15±0.03
3	164	stripped	0.08±0.04	0.07±0.02	3.21±0.03	0.04±0.02
4	164	stripped	0.33±0.03	0.26±0.03	2.75±0.03	1.25±0.02

In subject 1, the temperature change during CM excitation was 4.14°C in vivo and 6.02°C post-mortem. When the NM was implemented, a total temperature change of 0.38°C in vivo and 0.47°C post-mortem was observed. In the remaining three subjects, the temperature change in the CM ranged from 0.08°C to 0.39°C in vivo and 2.14°C to 3.21°C post-mortem. In the NM, the temperature change ranged from 0.07°C to 0.26°C in vivo and 0.04°C to 1.25°C post-mortem. In the case where an insulated tip guidewire was used, a very small temperature elevation was measured, 0.03±0.02°C in vivo and 0.06±0.04°C post-mortem, using the CM. The temperature at the tip of the guidewire was not observed to change during direct excitation.

In Figure 6, the instantaneous current on the guidewire at the current-sensor location is plotted along with the temperature at the guidewire tip. The time course is divided into four periods in which different mode settings and RF power levels were used. Periods A and B both used CM but with low average power (visualization) and high average power (heating test) sequences, respectively. Note that the current measurement relates to peak rather than average power, so it can be high even in a low average power sequence as in period A. The slight increase in measured current during period A can be attributed to an adjustment made to the amplitude of the output of the pTx system prior to beginning the heating test in period B. During period A (low average power) no temperature change was detected, while in period B (high average power) a temperature increase of ~4°C was observed. During period C the NM excitation led to negligible measured current, and the observed heating fell to ~0.5°C while still operating at high average power. In period D the RF power was shut off and the temperature returned to baseline.

3.4 In vivo Visualization

Figure 7A shows an example of CM visualization with ssTSE, from subject 1 in sagittal view. Although the guidewire is visible, the SNR is low and the signal fades towards the guidewire tip; with bright regions coming from the proximity to anterior and posterior coil arrays. In the other 3 subjects that used either the 164cm or 260cm length guidewires, the achieved contrast was even less to the point that the wires were not visible. For this reason, the direct excitation method (using the toroidal current sensor to excite the guidewire) was used as an alternate. Figure 7B shows a sagittal image acquired with bSSFP in subject 4. The guidewire is visualized with signal present from surrounding anatomy. In Figure 7C, a four-chamber view of the heart is shown, acquired with the bSSFP using B_1-shimmed NM excitation. The same view is shown in Figure 7D, also acquired with bSSFP but with direct excitation of the guidewire, using approximately 12W average RF power. In this view, the guidewire is hyperintense in the location of the right ventricle, while it is hypointense on Figure 7C.

To better understand the limitation in the CM visualization, we pulled the guidewire out in 10 cm intervals twice and took a ssTSE image at each interval position, using the CM in subject 4 (see Supporting Information Video S1). In Supporting Information Figure S3, images are

shown for three different insertions lengths. It is evident that reducing the insertion length leads to clearer visualization using this method.

Figure 8 shows an example of measured coupling **C** (Figures 8A&B) for two positions acquired about 15 seconds apart as the guidewire was retracted by approximately 5cm within the heart of one subject while acquiring NM anatomical images. It can be seen that the measured induced current in the NM remains low (Figure 8D) in both cases, despite the distribution of coupling across the channels and the total strength of coupling (Figure 8C) changing significantly in this time.

4 Discussion

This work demonstrated *in vivo* interventional MRI using a dynamically controlled auxiliary pTx system attached to a conventional MRI scanner, using current sensor measurements as active feedback. Structural MRI using standard sequences was shown to be possible with a standard nitinol guidewire in place with <1°C heating observed even when insulation was stripped from the guidewire tip to create worst-case conditions. Visualization of the guidewire itself using pTx coupling modes was easily achieved in phantom experiments (Figure 3B) where the overall extent of the guidewire shaft was nicely visualized in the FOV, in accordance with previous reports from ourselves (26) and others(13), but proved to be more challenging in vivo (Figure 7). However, in separate testing using direct low power excitation via the sensor coil and the cardiac array as a receiver, much more effective guidewire visualization was achieved in vivo, and this suggests a potentially useful approach worthy of further investigation. Visualization and heating in phantom tests were generally more extreme than that seen in vivo.

Structural images in vivo were generally artefact free, but some image non-uniformity was observed, with brightness decreasing quickly away from the surface of the body (Figure 4 and Figure 7C). This is to be expected since the surface transmit-receive coil produces a less uniform field than a body transmitter and receiver sensitivities of the array were not compensated in reconstruction. We also noted that the shape of the sheep's torso being rather peaked on the anterior side led to non-uniform loading of the coil, exacerbating this

effect; measured B_1^+ fields (Figure 5) were variable in their overall uniformity. We expect this would be reduced in a human torso with some optimization (40). Further development might improve imaging performance by including additional receive-only elements to improve signal reception. The coil array design focus in this work was on RF coupling control.

CM excitation in phantom experiments was observed to create large temperature increases, which were effectively nulled when operating in NM, as expected. In subjects 3 and 4 small temperature differences between the CM and NM were seen in vivo, but no unsafe conditions (heating>1°) were observed even for high-power scans. Heating tests in vivo showed systematically lower temperature increases than phantom tests; significant increases were only detected for stripped wires post-mortem, in three out of four cases. The explanation for this latter result is that the cooling effect of blood flow masked any temperature change *in vivo*, as also reported by Campbell-Washburn et al (6). Small temperature increases (0.5°C-1.25°C after 6 minutes) were seen when using NM excitation; this was also seen in phantom tests. This effect likely occurs because the current sensor was located outside the phantom/animal and hence may not fully characterize the currents present at the guidewire tip. Similar results were reported in phantoms (20) where performance was improved by adding a second current measurement inside the phantom using a B_1-map-based approach. Use of MRI to obtain the second current measurement has the disadvantage of requiring an interruption to continued imaging, which motivates the use of external sensors as in this work. In a preliminary study we have investigated alternative current sensor placement strategies (41) and found that a single external current-sensor could reduce the heating effect for all scenarios. In subject 1 the temperature change with the CM was the largest. We believe this was because a shorter guidewire was used, which might be closer to the resonant length (2).

Another key observation from our study was that unmodified (i.e. 'insulated tip') wires did not generate any observed unsafe conditions. The presence of an insulating polyurethane layer would be expected to reduce heating at the tip – similar results were reported in (6). However, that study did still show heating effects for 'insulated' wires at 'normal' SAR levels, while our experiments did not. Potential temperature increases could have been masked by blood flow, though another explanation may be the use of a small local transmit array in this

work compared with a body birdcage coil in (6); preliminary evidence from a separate study at 3T also supports this hypothesis (42). The insertion length can also influence heating as it causes resonant length to change as shown by Yeung et al (22).

Temperature measurements were made only at the guidewire tip, as this is the location where the most heating is expected (2,21). This is particularly true for our configuration, since the local RF transmit coil has a small footprint and is far from the entry point of the guidewire into the body. Additionally, we evaluated the potential for heating in prior simulation studies and found that the dominant location for any heating effects was always the wire tip (41). Nevertheless, future evaluation prior to human use could aim to verify the lack of heating at other points such as the entry point.

Visualization of the guidewire by CM excitation produced variable results across animal subjects, though it was found to work robustly in phantoms (26). The guidewire was only weakly visualized in the first subject which used a shorter and stripped-end guidewire; in the remainder of subjects it was consistently not seen at all. The large difference between phantoms and *in vivo* could indicate systematic differences between the strength of the RF-induced currents. The mechanism for such differences is unknown but might be a consequence of the blood's high conductivity which may be behaving as a coaxial shield around the guidewire. In subjects 3 and 4, the direct excitation method provided consistent visualization of the guidewire. This method has been demonstrated previously (13) though in that case the toroid was also used for MR signal detection. The images obtained (Figure 7B) show strong signal from the guidewire, but also a significant degree of background signal, which was suspected to be due to coupling between guidewire and transmit coils since the latter were not detuned; interaction between these fields may also explain the transition from hyper- to hypo-enhancement of the wire when moving towards the tip (Figure 7B). A future improvement would be to add detuning circuitry, which we hypothesize would largely resolve this issue. Additionally, we have so far only tested direct excitation with wires with stripped tips; performance with fully insulated wires is a subject for further investigation.

In subject 4, we assessed the efficacy of CM visualization as the guidewire was pulled out of the body, and found it became better visualized as the internal length was shortened

(Supporting Information Figure S3). This implies that the inserted length influences the RF-induced currents on the guidewire and may also explain the differences in performance between the (larger) animal model and (smaller) phantom. This result also provides evidence that the coupling conditions will change during an intervention, supporting the need for active control as used in our device. Further, Figure 8 indicates that a relatively small change of position of a guidewire could lead to a change in relative coupling to different coil elements. Although temperature changes were validated with guidewires in fixed positions, active control using this system was previously tested and is described in (43).

Limitations and challenges for future human use

Although X-ray guidance was used to enable accurate positioning, the methods presented offer the potential to remove the need for X-rays if wires can be visualized robustly. As demonstrated direct excitation of the guidewire is a viable visualization technique.

A key limitation for safe use in humans is that the pTx system does not actively monitor SAR, and the fact that the scanner's RF output is independently amplified by our system means that the scanner's own SAR modelling is unable to track the true SAR either. This was acceptable for the purpose so far, but to be suitable for use on humans, monitoring of all RFPAs (amplitude and phase)(44) is needed.

In addition, before human use is possible the current sensors would need to be redesigned to either be sterilizable or disposable. A degree of further miniaturization would also be desirable to allow for multiple sensor readings to be taken simultaneously, potentially improving current nulling performance. The device has so far been tested using a single sensor with a single inserted guidewire – more complex interventions using multiple conductive guidewires or braided catheters may also need to be examined to allow more complex future use.

Finally, the system was controlled by a standard PC running MatLab which was sufficient for these experiments, though the lack of real-time operating system was a limitation that was overcome in our experiments by adding dead-time to allow for variable time delays.

5 Conclusion

In conclusion, we have demonstrated *in vivo* imaging of a standard guidewire using a dynamically controlled auxiliary pTx system combined with a conventional scanner. The system could provide safe anatomical imaging using standard protocols with adaptive RF-induced current control. We also demonstrated a fast-constrained RF shimming method with adaptive adjustment as the NM change. Overall the study provides evidence that it is feasible to deploy a pTx system added on to otherwise unmodified MRI systems for procedures with standard guidewires, and that active control can achieve and sustain null modes of operation that control guidewire currents while still allowing MR images to be obtained.

Acknowledgments

Funding for this project is provided by the Medical Research Council (MRC) developmental pathway funding (MR/N027949) and by the Wellcome/EPSRC Centre for Medical Engineering (WT 203148/Z/16/Z) and by the British Heart Foundation (FS/20/26/34952). This research was funded in whole or in part by the Wellcome Trust [WT 203148/Z/16/Z]. For the purpose of Open Access, the author has applied a CC BY public copyright licence to any Author Accepted Manuscript (AAM) version arising from this submission

References

1. Nitz WR, Oppelt A, Renz W, Manke C, Lenhart M, Link J. On the heating of linear conductive structures as guide wires and catheters in interventional MRI. J. Magn. Reson. Imaging 2001;13:105–114 doi: 10.1002/1522-2586(200101)13:1<105::AID-JMRI1016>3.0.CO;2-0.

2. Park SM, Kamondetdacha R, Nyenhuis JA. Calculation of MRI-induced heating of an implanted medical lead wire with an electric field transfer function. J. Magn. Reson. Imaging 2007;26:1278–1285 doi: 10.1002/jmri.21159.

3. Griffin GH, Anderson KJT, Celik H, Wright GA. Safely assessing radiofrequency heating potential of conductive devices using image-based current measurements. Magn. Reson. Med. 2015;73:427–441 doi: 10.1002/mrm.25103.

4. Nazarian S, Kolandaivelu A, Zviman MM, et al. Feasibility of real-time magnetic resonance imaging for catheter guidance in electrophysiology studies. Circulation 2008;118:223–229 doi: 10.1161/CIRCULATIONAHA.107.742452.

5. Campbell-Washburn AE, Tavallaei MA, Pop M, et al. Real-time MRI guidance of cardiac interventions. J. Magn. Reson. Imaging 2017:1–16 doi: 10.1002/jmri.25749.

6. Campbell-Washburn AE, Rogers T, Stine AM, et al. Right heart catheterization using metallic guidewires and low SAR cardiovascular magnetic resonance fluoroscopy at 1.5 Tesla: First in human experience. J. Cardiovasc. Magn. Reson. 2018;20:1–9 doi: 10.1186/s12968-018-0458-7.

7. Campbell-Washburn AE, Ramasawmy R, Restivo MC, et al. Opportunities in interventional and diagnostic imaging by using high-performance low-field-strength MRI. Radiology 2019;293:384–393 doi: 10.1148/radiol.2019190452.

8. Massmann A, Buecker A, Schneider GK. Glass-fiber-based MR-safe guidewire for MR imaging-guided endovascular interventions: In vitro and preclinical in vivo feasibility study. Radiology 2017.

9. Campbell-Washburn AE, Rogers T, Basar B, et al. Positive contrast spiral imaging for visualization of commercial nitinol guidewires with reduced heating. J. Cardiovasc. Magn. Reson. 2015;17:114 doi: 10.1186/s12968-015-0219-9.

10. Campbell-Washburn AE, Rogers T, Xue H, Hansen MS, Lederman RJ, Faranesh AZ. Dual echo positive contrast bSSFP for real-time visualization of passive devices during magnetic resonance guided cardiovascular catheterization. J. Cardiovasc. Magn. Reson. 2014;16:88 doi: 10.1186/s12968-014-0088-7.

11. Razavi R, Hill DLG, Keevil SF, et al. Cardiac catheterisation guided by MRI in children and adults with congenital heart disease. Lancet 2003;362:1877–1882 doi: 10.1016/S0140-6736(03)14956-2.

12. Wacker FK, Hillenbrand CM, Duerk JL, Lewin JS. MR-guided endovascular interventions: Device visualization, tracking, navigation, clinical applications, and safety aspects. Magn. Reson. Imaging Clin. N. Am. 2005;13:431–439 doi: 10.1016/j.mric.2005.04.004.

13. Etezadi-Amoli M, Stang P, Kerr A, Pauly J, Scott G. Interventional device visualization with toroidal transceiver and optically coupled current sensor for radiofrequency safety monitoring. Magn. Reson. Med. 2015;73:1315–1327 doi: 10.1002/mrm.25187.

14. Hillenbrand CM, Reykowski A, Wong EY, Rafie S, Nitz W, Duerk JL. The Bazooka Coil : A Novel Dual-Purpose Device for Active Visualization and Reduction of Cable Currents in Electrically Conductive Endovascular Instruments. Radiology 2005;8:2005.

15. Mckinnon GC, Debatin JF, Leung DA, Wildermuth S, Holtz DJ, Von Schulthess GK. Towards active guidewire visualization in interventional magnetic resonance imaging. MAGMA 1996;4:13–18.

16. Kocaturk O, Saikus CE, Guttman M a, et al. Whole shaft visibility and mechanical performance for active MR catheters using copper-nitinol braided polymer tubes. J. Cardiovasc. Magn. Reson. 2009;11:29 doi: 10.1186/1532-429X-11-29.

17. Ratnayaka K, Faranesh AZ, Guttman MA, Kocaturk O, Saikus CE, Lederman RJ. Interventional cardiovascular magnetic resonance: still tantalizing. J. Cardiovasc. Magn. Reson. 2008;10:62 doi: 10.1186/1532-429X-10-62.

18. Feng S, Qiang R, Kainz W, Chen J. A technique to evaluate MRI-induced electric fields at the ends of practical implanted lead. IEEE Trans. Microw. Theory Tech. 2015;63:305–313 doi: 10.1109/TMTT.2014.2376523.

19. Yeung CJ, Susil RC, Atalar E. RF heating due to conductive wires during MRI depends on the phase distribution of the transmit field. Magn. Reson. Med. 2002;48:1096–1098 doi: 10.1002/mrm.10310.

20. Etezadi-Amoli M, Stang P, Kerr A, Pauly J, Scott G. Controlling radiofrequency-induced currents in guidewires using parallel transmit. Magn. Reson. Med. 2015;74:1790–1802 doi: 10.1002/mrm.25543.

21. Gudino N, Sonmez M, Yao Z, et al. Parallel transmit excitation at 1.5 T based on the minimization of a driving function for device heating. Med. Phys. 2015;42:359–371 doi: 10.1118/1.4903894.

22. Yeung CJ, Karmarkar P, McVeigh ER. Minimizing RF heating of conducting wires in MRI.

Magn. Reson. Med. 2007;58:1028–1034 doi: 10.1002/mrm.21410.

23. Armenean C, Perrin E, Armenean M, Beuf O, Pilleul F, Saint-Jalmes H. RF-induced temperature elevation along metallic wires in clinical magnetic resonance imaging: Influence of diameter and length. Magn. Reson. Med. 2004;52:1200–1206 doi: 10.1002/mrm.20246.

24. McElcheran CE, Golestanirad L, Iacono MI, et al. Numerical Simulations of Realistic Lead Trajectories and an Experimental Verification Support the Efficacy of Parallel Radiofrequency Transmission to Reduce Heating of Deep Brain Stimulation Implants during MRI. Sci. Rep. 2019;9:1–14 doi: 10.1038/s41598-018-38099-w.

25. Eryaman Y, Guerin B, Akgun C, et al. Parallel transmit pulse design for patients with deep brain stimulation implants. Magn. Reson. Med. 2015;73:1896–1903 doi: 10.1002/mrm.25324.

26. Godinez F, Scott G, Padormo F, Hajnal J V., Malik SJ. Safe guidewire visualization using the modes of a PTx transmit array MR system. Magn. Reson. Med. 2020;83:2343–2355 doi: 10.1002/mrm.28069.

27. Overall WR, Pauly JM, Stang PP, Scott GC. Ensuring safety of implanted devices under MRI using reversed RF polarization. Magn. Reson. Med. 2010;64:823–833 doi: 10.1002/mrm.22468.

28. Eryaman Y, Turk EA, Oto C, Algin O, Atalar E. Reduction of the radiofrequency heating of metallic devices using a dual-drive birdcage coil. Magn. Reson. Med. 2013;69:845–52 doi: 10.1002/mrm.24316.

29. Orzada S, Solbach K, Gratz M, et al. A 32-channel parallel transmit system add-on for 7T MRI Deniz CM, editor. PLoS One 2019;14:e0222452 doi: 10.1371/journal.pone.0222452.

30. Feng K, Hollingsworth NA, McDougall MP, Wright SM. A 64-channel transmitter for investigating parallel transmit MRI. IEEE Trans. Biomed. Eng. 2012;59:2152–2160 doi: 10.1109/TBME.2012.2196797.

31. Winter L, Silemek B, Petzold J, et al. Parallel transmission medical implant safety testbed: Real-time mitigation of RF induced tip heating using time-domain E-field sensors. Magn. Reson. Med. 2020;84:3468–3484 doi: 10.1002/mrm.28379.

32. Godinez F, Tomi-Tricot R, Barthel M, et al. An 8 channel parallel transmit system with current sensor feedback for MRI-guided interventional applications. arXiv Prepr. arXiv2103.10399 2021.

33. Zanchi MG, Venook R, Pauly JM, Scott GC. An optically coupled system for quantitative monitoring of MRI-induced RF currents into long conductors. IEEE Trans. Med. Imaging 2010;29:169–178 doi: 10.1109/TMI.2009.2031558.

34. Padormo F, Beqiri A, Hajnal J V., Malik SJ. Parallel transmission for ultrahigh-field imaging. NMR Biomed. 2016;29:1145–1161 doi: 10.1002/nbm.3313.

35. Ladd ME, Quick HH. Reduction of resonant RF heating in intravascular catheters using coaxial chokes. Magn. Reson. Med. 2000;43:615–619 doi: 10.1002/(SICI)1522-2594(200004)43:4<615::AID-MRM19>3.0.CO;2-B.

36. Pictet J, Meuli R, Wicky S, Van Der Klink JJ. Radiofrequency heating effects around resonant lengths of wire in MRI. Phys. Med. Biol. 2002;47:2973–2985 doi: 10.1088/0031-9155/47/16/312.

37. Klose U. Mapping of the radio frequency magnetic field with a MR snapshot FLASH technique. Med. Phys. 1992;19:1099–1104 doi: 10.1118/1.596828.

38. Brunner DO, Pruessmann KP. B 1 Interferometry for the Calibration of RF Transmitter Arrays. 2009;1488:1480–1488 doi: 10.1002/mrm.21893.

39. ASTM standard F 2182-2002a. Standard test method for measurement of radio frequency induced heating near passive implants during magnetic resonance imaging. ASTM Int. 2011:1–14 doi: 10.1520/F2182-11A.1.7.

40. Weinberger O, Winter L, Dieringer MA, et al. Local Multi-Channel RF Surface Coil versus Body RF Coil Transmission for Cardiac Magnetic Resonance at 3 Tesla: Which Configuration Is Winning the Game? PLoS One 2016.

41. Graesslin I, Homann H, Biederer S, et al. A specific absorption rate prediction concept for parallel transmission MR. Magn. Reson. Med. 2012;68:1664–1674.

42. Godinez F, Scott G, Hajnal J V., Malik SJ. Is a Local Tx Coil Sufficient for Guidewire Safety in MRI? In: Proc. Intl. Soc. Mag. Reson. Med. 29. Vancouver Canada: ISMRM; 2021.

43. Godinez F, Hajnal J V, Malik SJ. Auxiliary PTx system for active control of induced RF currents in conductive guidewires. In: Proc. Intl. Soc. Mag. Reson. Med. 27. ; 2019.

44. Zhu Y, Alon L, Deniz CM, Brown R, Sodickson DK. System and SAR characterization in parallel RF transmission. Magn. Reson. Med. 2012;67:1367–1378 doi: 10.1002/mrm.23126.

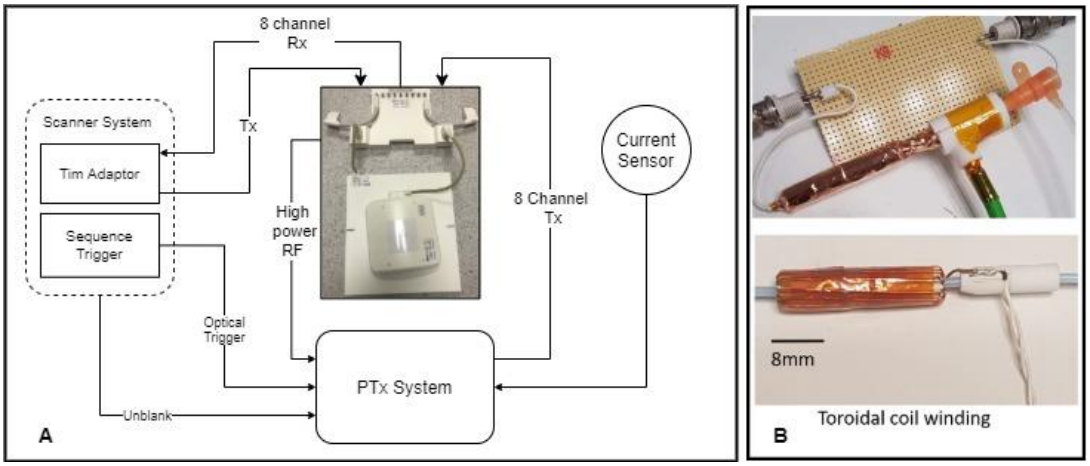

Figure 1: Block schematic of (A) system signal flow and (B) current sensor construction. Acronyms: RF power amplifier (RFPA), National Instruments (NI), Total imaging matrix (Tim).

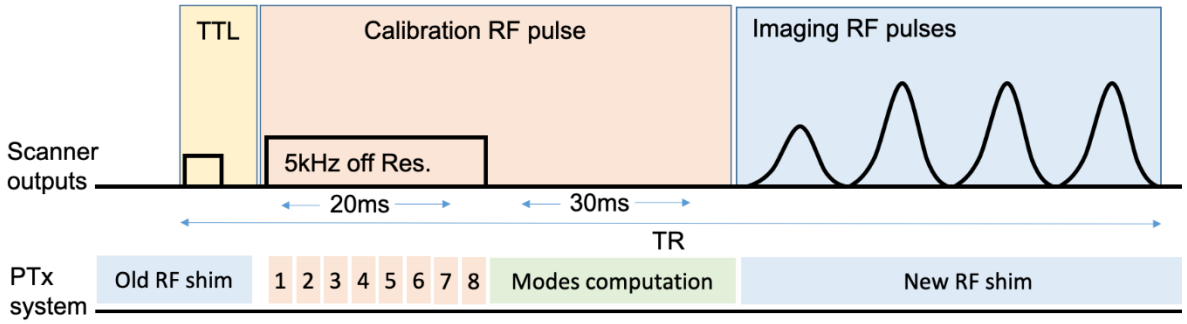

Figure 2 Timing diagram of the pulse sequence implementation of the coupling calibration process with subsequent imaging pulse sequence (TSE is shown here as an example). The same calibration phase was used for the bSSFP sequence.

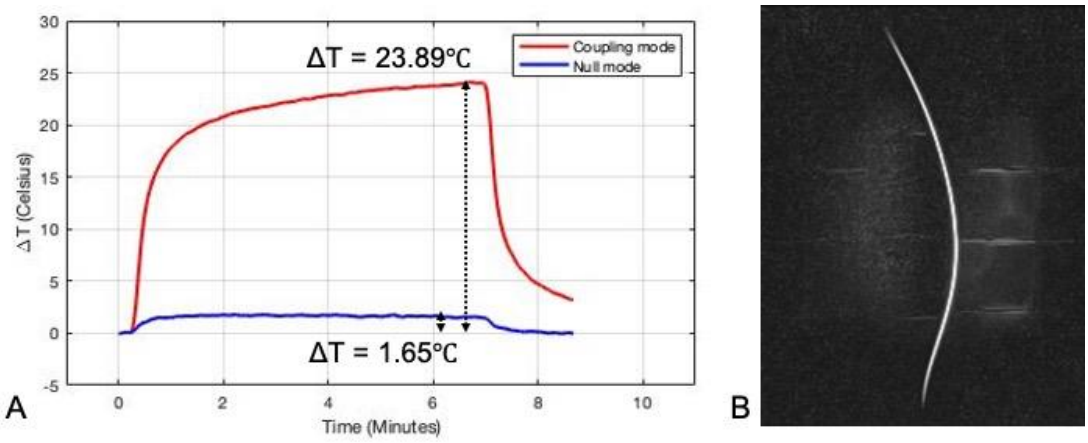

Figure 3 A) Phantom heating tests with the CM or NM and the bSSFP pulse sequence. B) Guidewire visualization with CM using ssTSE pulse sequence.

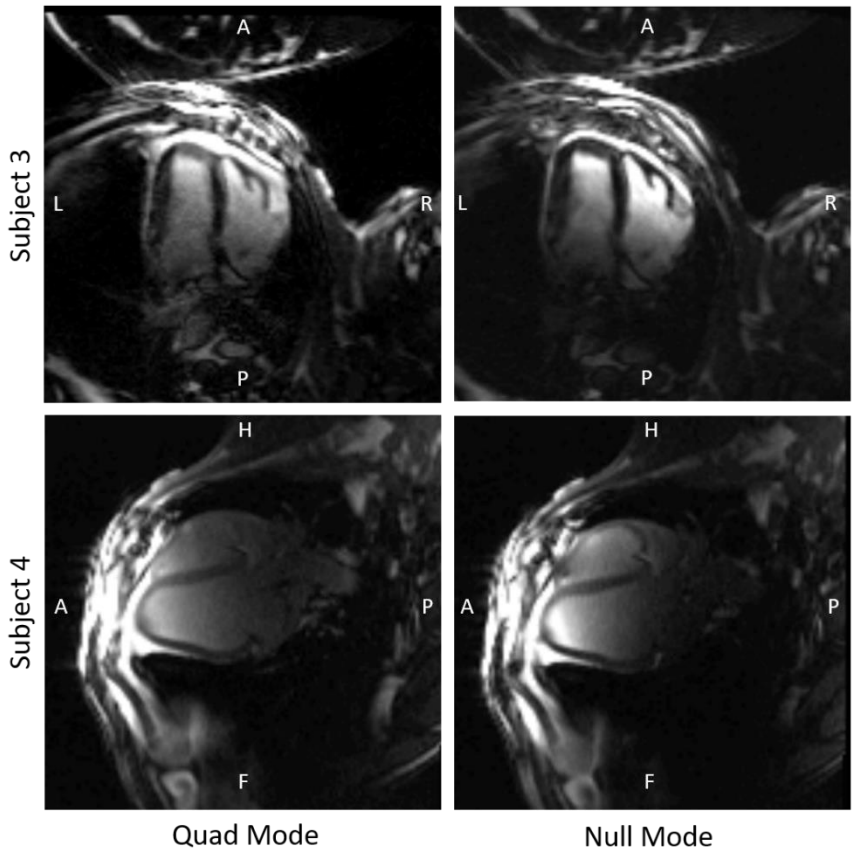

Figure 4 Four-chamber view of heart anatomy with the guidewire inserted in the right ventricle. (left) The quad mode with B1 shimming was used and is compared to (right)

the Null mode case. The left ventricle long axis of the heart is shown in the top row in an axial view for subject 3 and the bottom row in a sagittal view for subject 4.

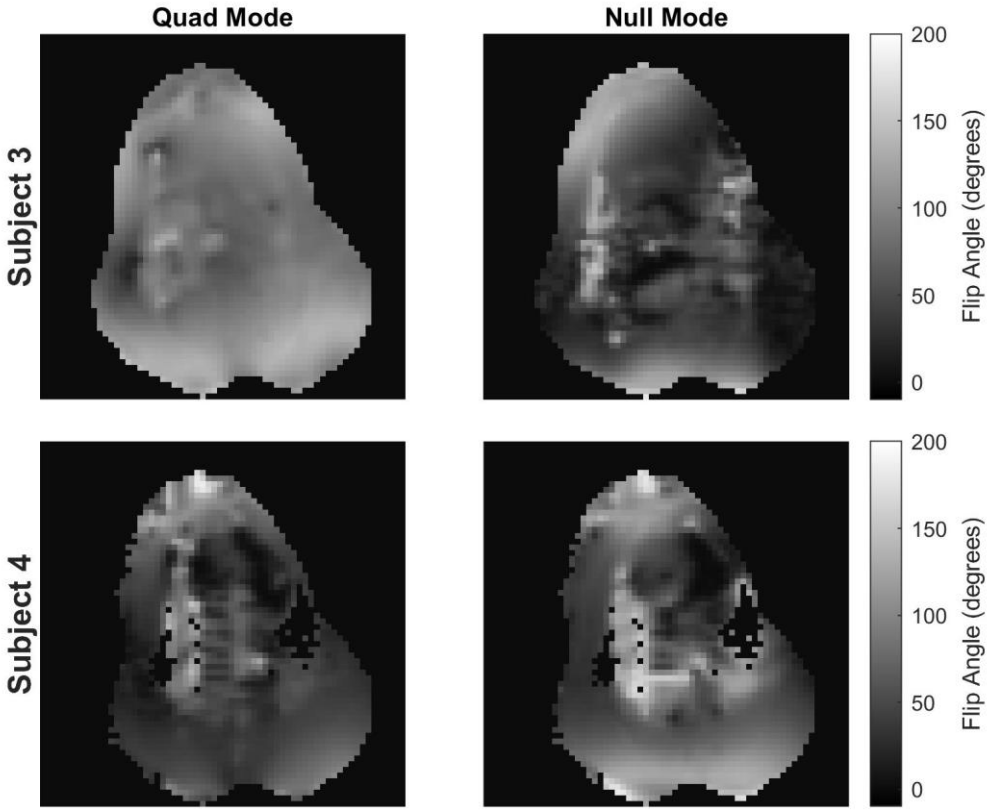

Figure 5 B_1^+ (flip angle) maps for subjects 3 and 4 in quad and null mode (nominal flip angle 80°). The axial plane is shown in all maps.

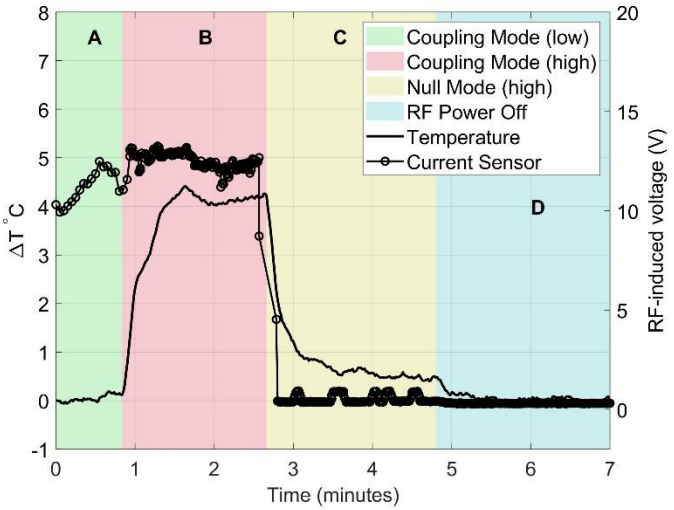

Figure 6 Temperature and instantaneous current sensor measurements during a heating test on subject 1. The current sensor is not calibrated hence the display shows induced voltage in the units measured from the ADC. This measurement trace is divided into four regions, marking different times during this experiment. During period A the scanner is executing a low average power scan in CM, switching to high average power in period B; temperature increases in this mode. During period C the high power is maintained but switched from CM to NM – the measured induced current at the sensor and the temperature at the tip of the wire both drop. During period D the RF power amplifiers were switched off.

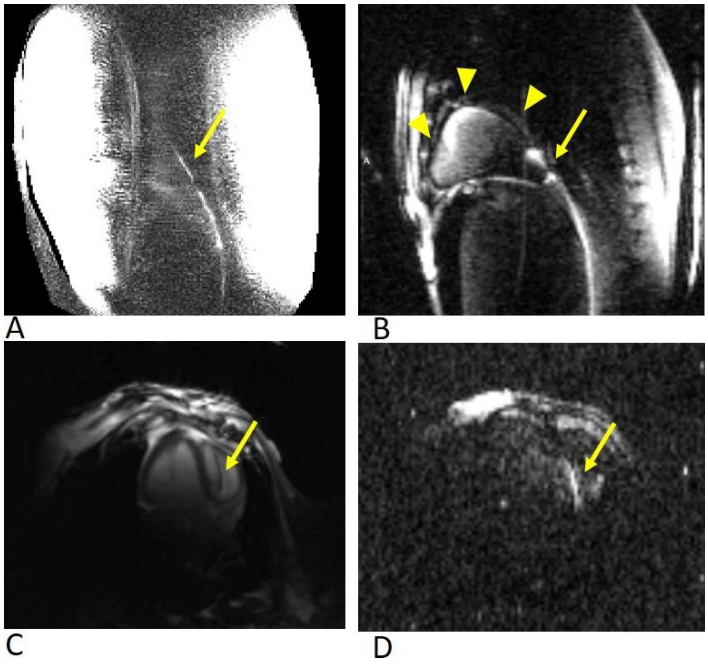

Figure 7 A) Guidewire visualization using the low-power ssTSE sequence in coupling mode with pTx in subject 1. B) Guidewire visualization using the direct excitation method using the bSSFP in subject 4. C) A four-chamber view with a bSSFP sequence in the same subject, while operating with the null mode. D) The same four-chamber view of the heart during direct guidewire excitation, placed in the right ventricle. The wire is indicated by the arrow and triangles indicate the distal end of the guidewire.

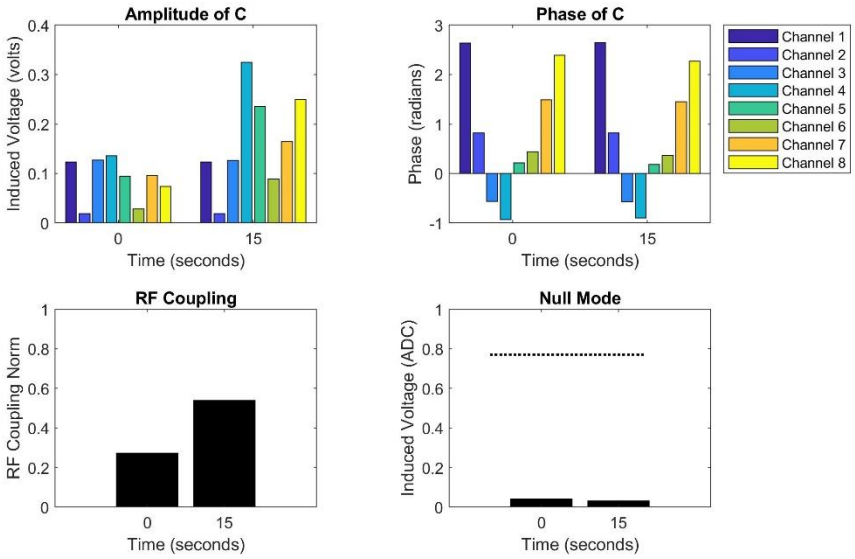

Figure 8 (A&B): Magnitude (A) and phase (B) of the measured coupling **C** between each channel and a guidewire placed within the heart of Subject 4. These measurements were acquired approximately 15 seconds apart as the wire was retracted by about 5cm. The measured coupling to each channel and the total coupling (defined as $\|\boldsymbol{C}\|$) changes substantially. (D): the measured current when applying a null mode excitation at these two positions remained low.

Figure Captions

Figure 9 Block schematic of (A) system signal flow and (B) current sensor construction. Acronyms: RF power amplifier (RFPA), National Instruments (NI), Total imaging matrix (Tim).

Figure 10 Timing diagram of the pulse sequence implementation of the coupling calibration process with subsequent imaging pulse sequence (TSE is shown here as an example). The same calibration phase was used for the bSSFP sequence.

Figure 11 A) Phantom heating tests with the CM or NM and the bSSFP pulse sequence. B) Guidewire visualization with CM using ssTSE pulse sequence.

Figure 12 Four-chamber view of heart anatomy with the guidewire inserted in the right ventricle. (left) The quad mode with B1 shimming was used and is compared to (right) the Null mode case. The left ventricle long axis of the heart is shown in the top row in an axial view for subject 3 and the bottom row in a sagittal view for subject 4.

Figure 13 B_1^+ (flip angle) maps for subjects 3 and 4 in quad and null mode (nominal flip angle 80°). The axial plane is shown in all maps.

Figure 14 Temperature and instantaneous current sensor measurements during a heating test on subject 1. The current sensor is not calibrated hence the display shows induced voltage in the units measured from the ADC. This measurement trace is divided into four regions, marking different times during this experiment. During period A the scanner is executing a low average power scan in CM, switching to high average power in period B; temperature increases in this mode. During period C the high power is maintained but switched from CM to NM – the measured induced current at the sensor and the temperature at the tip of the wire both drop. During period D the RF power amplifiers were switched off.

Figure 15 A) Guidewire visualization using the low-power ssTSE sequence in coupling mode with pTx in subject 1. B) Guidewire visualization using the direct excitation method using the bSSFP in subject 4. C) A four-chamber view with a bSSFP sequence in the same subject, while operating with the null mode. D) The same four-chamber view of the heart during direct guidewire excitation, placed in the right ventricle. The wire is indicated by the arrow and triangles indicate the distal end of the guidewire.

Figure 8. (A&B): Magnitude (A) and phase (B) of the measured coupling **C** between each channel and a guidewire placed within the heart of Subject 4. These measurements were acquired approximately 15 seconds apart as the wire was retracted by about 5cm. The measured coupling to each channel and the total coupling (defined as $\|\boldsymbol{C}\|$) changes substantially. (D): the measured current when applying a null mode excitation at these two positions remained low. The dashed line is the value when the coupling mode is selected.

Supporting information Captions

Supporting Information Figure S1. User interface to control the pTx system.

Supporting Information Figure S2. Temperature profile during a post-mortem heating test in subject 4 using the coupling mode.

Supporting Information Figure S3. Guidewire pull starting from the left to the right. At each position, the guidewire was pulled out about 10 cm. The arrow indicates the location of the guidewire. On the final retraction the coil array was shifted towards the hind legs so that the FOV could cover most of the inserted length.

Supporting Information video S2. Video of guidewire being pulled out during direct excitation visualization. Video displayed at 15 frames per second.